

Analysis of nonharmonic oscillations in Schottky diodes.D. Pardo,^{1, a)} J. Grajal,^{1, b)} S. Pérez,² T. González,² and J. Mateos²

¹⁾*Department of Signals, Systems and Radiocommunications. ETSIT, Technical University of Madrid, Av. Complutense 30. 28040 Madrid, Spain*

²⁾*Department of Applied Physics. University of Salamanca, Plaza de la Merced s/n. 37008 Salamanca, Spain*

(Dated: 2 September 2013)

We investigate damped nonharmonic oscillations at terahertz frequencies observed in the current response of Schottky diodes simulated with the Monte Carlo method under applied signals of a few hundred GHz. From Monte Carlo simulations of different diode structures, two kinds of nonharmonic oscillations have been identified. The first kind of oscillations is due to the coupling of the nonlinear performance of the Schottky junction with the inertial motion of the carriers in the non-depleted region of the epilayer. The second kind of oscillations is due to the modulation of the $n^+ - n$ junction when high electric fields are induced in the non-depleted region of the epilayer. These oscillations constitute a promising mechanism for THz signal generation.

^{a)}Electronic mail: dpardo@gmr.ssr.upm.es.

^{b)}Electronic mail: jesus@gmr.ssr.upm.es.

I. INTRODUCTION

Schottky barrier diodes have been widely studied because they exhibit a rich variety of nonlinear physical phenomena and they offer the possibility of efficient frequency multiplication and mixing at THz band¹⁻⁴.

From Monte Carlo (MC) simulations of Schottky diodes under time varying excitations of a few hundred GHz, we have observed the generation of damped nonharmonic oscillations (*NHOs*) of terahertz frequencies in the current response of this device.

The MC simulations of homogeneous diodes (Schottky diodes with substrate doping equal to the epilayer doping, denoted by HSBD) and Schottky diodes with $n^+ - n$ junction (Schottky diodes with substrate doping different from the epilayer doping, denoted by SBDs) have shown the existence of two kinds of *NHOs*. While the first kind is common to both devices, the second kind only appears in SBDs when very high electric fields are generated in the non-depleted region of the epilayer.

Some publications based on MC simulations of Schottky diodes^{5,6} show *NHOs*. However, none of these publications have paid attention to these oscillations.

Nonharmonic oscillations with similar characteristics to the *NHOs* have been theoretically predicted in the solution of nonlinear systems. In most cases it is impossible to solve analytically such systems in terms of elementary functions. Ref. 7 analyses a simple damped nonharmonic oscillator, showing that the nonlinearity modifies the restoring force of the physical system and, hence, the period of the oscillator changes with the amplitude of the oscillation.

On the other hand, the theoretical examination of series RLC circuits with nonlinear elements has shown the existence of stable nonharmonic oscillatory solutions similar to the *NHOs* that we have found in Schottky diodes^{8,9}.

The terahertz sources with adequate power, frequency agility, and spectral purity are the most difficult challenge facing terahertz frequency engineers⁴. *NHOs* can be promising for harmonic generation at terahertz bands. The waveforms of *NHOs* in Schottky diodes are similar to the step-like waveforms generated by step recovery diodes¹⁰⁻¹⁴ or nonlinear transmission lines^{15,16}. All of them present a rich harmonic content at THz frequencies which can be used in comb generators.

The aim of this work is to analyse and interpret the *NHOs* obtained from Monte Carlo

simulations of GaAs Schottky diodes under certain time varying excitations. We have used an analytical model for the carrier transport based on the momentum balance equation to gain physical insight on the origin of these oscillations¹⁷. Simpler current relations based on the drift-diffusion model are not able to predict the *NHOs*. On the other hand, a lumped-element equivalent circuit model is also able to describe the *NHOs*, what eases the analysis of these oscillations in complex circuits.

The paper begins with the description of the main features of the *NHOs* obtained from MC simulation of GaAs Schottky diodes. Section III is devoted to the mathematical models for interpreting the results from the simulations. The interpretation of the features of the *NHOs* is presented in Section IV. Some conclusions are drawn in Section V.

II. DESCRIPTION OF THE *NHOs*

This section describes the main features of the *NHOs* observed in the current response of GaAs SBDs simulated with the MC method under sinusoidal applied signals $V_{app}(t) = V_0 + V_1 \sin(2\pi ft)$ (denoted by (V_0, V_1, f)).

An ensemble MC self-consistently coupled with a one dimensional Poisson solver is employed. The effect of degeneracy is accounted for by locally using the classical rejection technique^{18,19}. The ohmic contact is modeled as a surface that injects carriers in thermal equilibrium with the lattice (in order to maintain the neutrality in the region very close to the contact) according to Fermi-Dirac statistics. In addition, any carrier reaching this contact leaves the device. On the other hand, the Schottky contact is simulated as a perfect absorbent surface. Scattering mechanisms included in the Monte Carlo simulator are ionized impurities, acoustic phonon, polar and non-polar optic phonon and intervalley mechanisms. The band structure is modeled as a conduction band with three spherical non-parabolic valleys¹⁸. The charge density is updated every 0.5 fs and devices are divided into cells of 20 Å.

The characteristics of the Schottky diodes taken as a reference for this study are presented in Table I. The ideal barrier height selected is 0.99 V, the anode area 0.9 μm^2 and the temperature 300 K.²⁰

TABLE I. Schottky diodes analysed.

	Doping, (cm^{-3})		Length, (nm)	
	Epilayer	Substrate	Epilayer	Substrate
HSBD	5×10^{17}	5×10^{17}	200	50
SBD	5×10^{17}	2×10^{18}	200	50

A. *NHOs* in homogeneous Schottky diodes

Figs. 1 shows the current response obtained from the MC simulation of the reference HSBD under $(-3.0 \text{ V}, 3.85 \text{ V}, f)$ for different frequencies of the applied signal f . *NHOs* appear when the depletion region width is close to its minimum for frequencies higher than 100 GHz and they tend to disappear when f is higher than 550 GHz.

To understand why the oscillations observed in Figs. 1 vanish under $(-3.0 \text{ V}, 3.85 \text{ V}, f)$ with $f > 550 \text{ GHz}$, Fig. 2 shows the evolution of width of the depletion region in a period of the applied signals. The frequency f for which the *NHOs* disappear corresponds to the reduction of the swing of the edge of the depletion region with respect to the swing at lower frequencies due to the saturation of the electron velocity^{21,22}.

An estimate of the oscillation frequencies in the time domain is shown in Table II (the analysis of the *NHOs* in the frequency domain is carried out in Subsection IIC). The frequency of the first $f_{NHO(1)}$, second $f_{NHO(2)}$ and third $f_{NHO(3)}$ periods shown in this table are obtained as the inverse of the time separation between two consecutive minima of the *NHOs*. Table II shows that the frequency $f_{NHO(i)}$ of the successive periods of the *NHOs* varies with time, a characteristic performance of the damped nonharmonic oscillations⁷. On the other hand, $f_{NHO(i)}$ increases with the frequency of the applied signal.

B. *NHOs* in $n^+ - n$ Schottky diodes

Fig. 3 presents the current response of the reference SBD under $(-3.0 \text{ V}, 3.85 \text{ V}, f)$. *NHOs* appear for $f > 100 \text{ GHz}$ with features similar to the *NHOs* of the reference HSBD ($f_{NHO(i)}$, $i = 1, 2, 3$ in Tables II for HSBDs and III for SBDs). When the frequency of the applied signal is higher than 600 GHz, Fig. 4 shows that the velocity of the electrons in the epilayer saturates and the *NHOs* disappear. However, for $f > 600 \text{ GHz}$, Fig. 3 shows *NHOs*

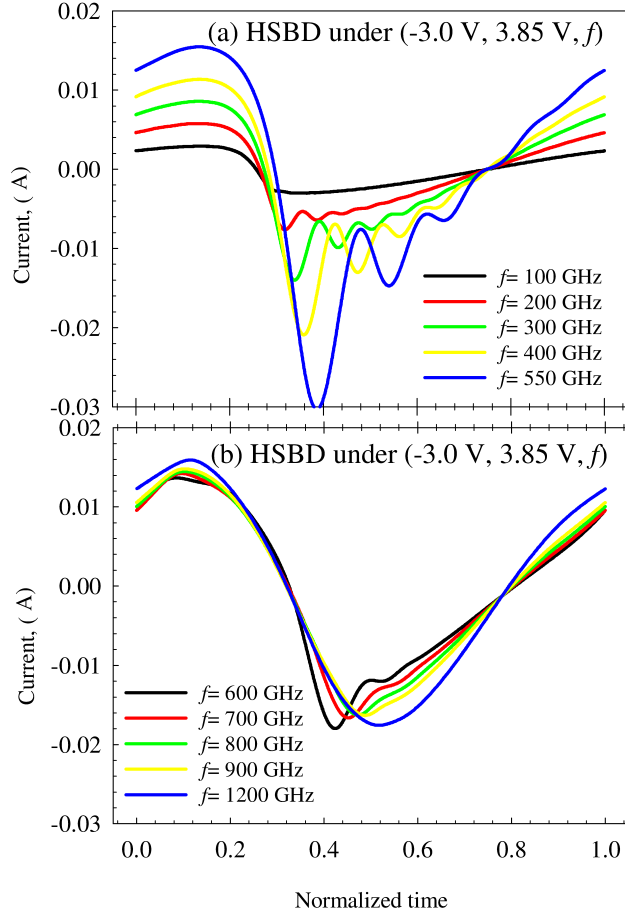


FIG. 1. Current response obtained from the MC simulation of the reference HSB under (-3.0 V, 3.85 V, f).

TABLE II. Frequency of the first, second and third periods of the NHO s directly measured from the time domain current response of the reference HSB under applied signals (-3.0 V, 3.85 V, f) simulated with MC.

f , (GHz)	$f_{NHO(1)}$, (THz)	$f_{NHO(2)}$, (THz)	$f_{NHO(3)}$, (THz)
200	2.95	3.76	5.12
300	3.22	4.16	5.12
400	3.47	4.49	5.30
500	3.60	4.67	—
550	3.58	4.73	—
600	—	—	—

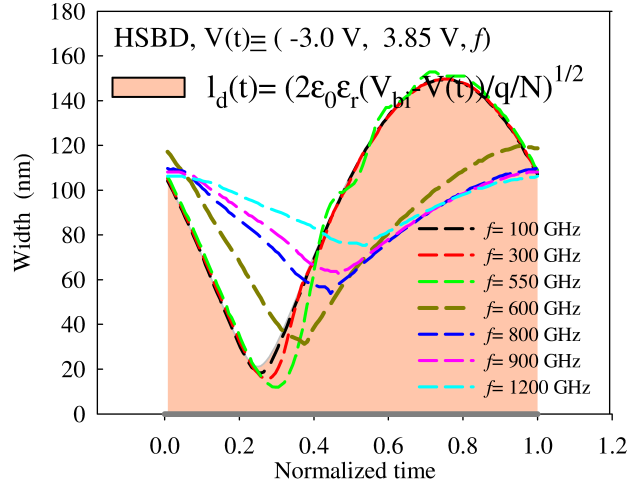


FIG. 2. Time evolution of the width of the depletion region of the reference HSBD under $(-3.0 \text{ V}, 3.85 \text{ V}, f)$ obtained from MC simulations. The width has been evaluated at the position where the charge carriers concentration falls to $0.6 N_e$.

of lower amplitude and higher frequency than the *NHOs* observed for lower frequencies of the applied signal. Therefore, we can distinguish between two kind of *NHOs*, the first kind due to physical processes in the epilayer since they are observed both in HSBD and SBD, and the second kind due to physical processes in the substrate or to some coupling between the epilayer and the substrate: The second kind of *NHOs* do not exist for HSBDs, so they involve necessarily the substrate.

Table III for the reference SBD shows that the frequency of the two kinds of *NHOs* increases with the frequency of the applied signal. The same dependence was observed in Table II for the first kind of *NHOs* in the reference HSBD. However, the frequency of these oscillations is a few hundred GHz larger for the SBD (epilayer length 200 nm) than that for the HSBD (epilayer length 250 nm). The simulation of the HSBD with epilayer length equal to 200 nm leads to frequencies for the first kind of *NHOs* closer to the frequency of these oscillations in the reference SBD, see Table IV. The comparison of Tables III and IV indicates that the presence of the substrate on the SBD also affects the frequency of the first kind of *NHOs*.

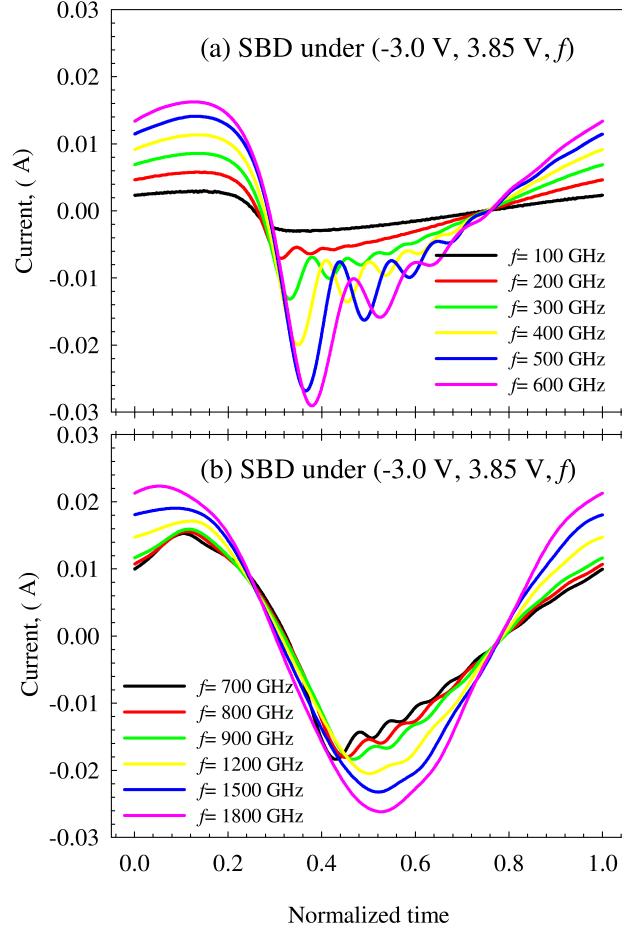


FIG. 3. Current response obtained from the MC simulation of the reference SBD under $(-3.0 \text{ V}, 3.85 \text{ V}, f)$.

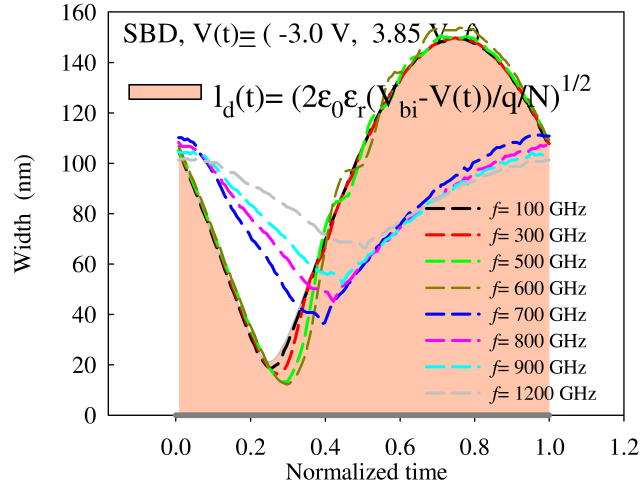


FIG. 4. Time evolution of the width of the depletion region of the reference SBD under $(-3.0 \text{ V}, 3.85 \text{ V}, f)$ obtained from MC simulations.

TABLE III. Frequency of the first, second and third periods of the $NHOs$ directly measured from the time domain current response of the reference SBD under applied signals (-3.0 V, 3.85 V, f) simulated with MC.

f , (GHz)	$f_{NHO(1)}$, (THz)	$f_{NHO(2)}$, (THz)	$f_{NHO(3)}$, (THz)
200	3.29	3.98	5.25
300	3.53	4.44	5.34
400	3.81	4.90	5.69
500	3.99	5.22	6.01
600	4.12	5.66	–
700	9.13	11.29	11.39
800	10.71	11.54	11.62
900	11.80	11.97	–
1200	–	–	–

TABLE IV. Frequency of the first, second and third periods of the $NHOs$ directly measured from the time domain current response of the reference HSBD defined in Table I but with epilayer length of 200 nm under applied signals (-3.0 V, 3.85 V, f) simulated with MC.

f , (GHz)	$f_{NHO(1)}$, (THz)	$f_{NHO(2)}$, (THz)	$f_{NHO(3)}$, (THz)
200	3.12	4.31	–
300	3.49	4.50	5.74
400	3.72	5.00	6.53
500	3.95	5.15	–

C. Spectra of $NHOs$

Figs. 5 and 6 show the spectra of the current response presented in Figs. 1 and 3 for the reference HSBD and SBD, respectively. The $NHOs$ are localised in a short time span of the current response of the diodes, and, therefore, their spectral content is very broadband.

For frequencies of the applied signals $f \lesssim 600$ GHz, the first kind of $NHOs$ (the only

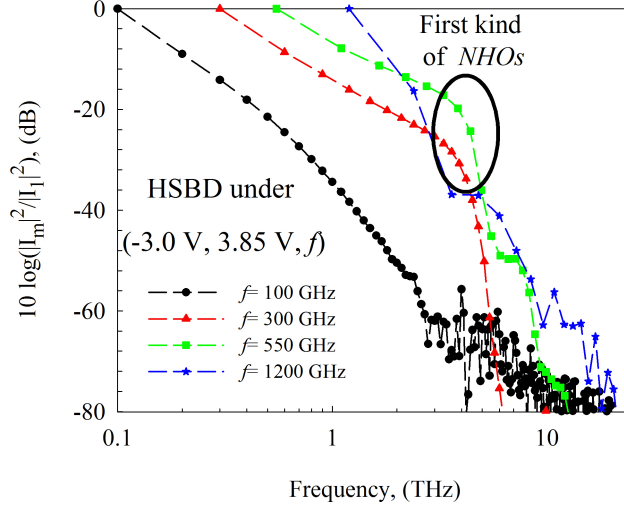


FIG. 5. Spectra of the current response presented in Fig. 1 for the reference HSBD (fast Fourier transform of the current), normalized to the module of the fundamental harmonic of the currents I_1 . The sampling frequency for each spectrum is the frequency of the applied signal.

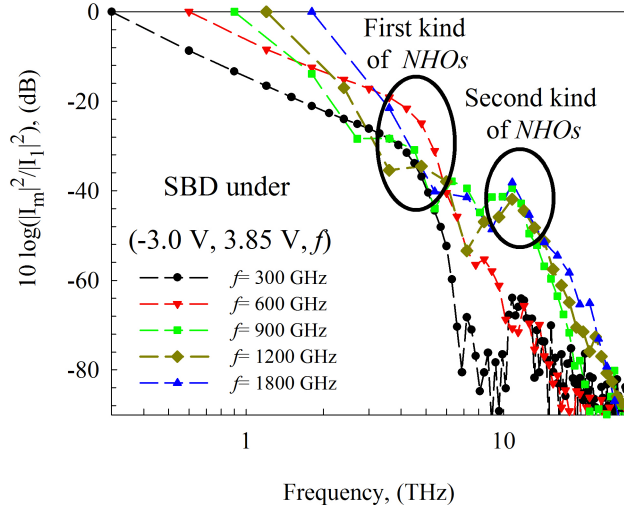


FIG. 6. Spectra of the current response presented in Figs. 3 for the reference SBD (fast Fourier transform of the current), normalized to the module of the fundamental harmonic of the currents I_1 . The sampling frequency for each spectrum is the frequency of the applied signal.

kind of *NHOs* excited at these frequencies) is detected in the spectra by the abrupt decay of the amplitude of the fast Fourier transform at frequencies between $f_{NHO(1)}$ and $f_{NHO(2)}$ for both HSBDs and SBDs. This is observed from the comparison of the spectra of Figs. 5 and 6 with the corresponding time domain data of Tables II and III.

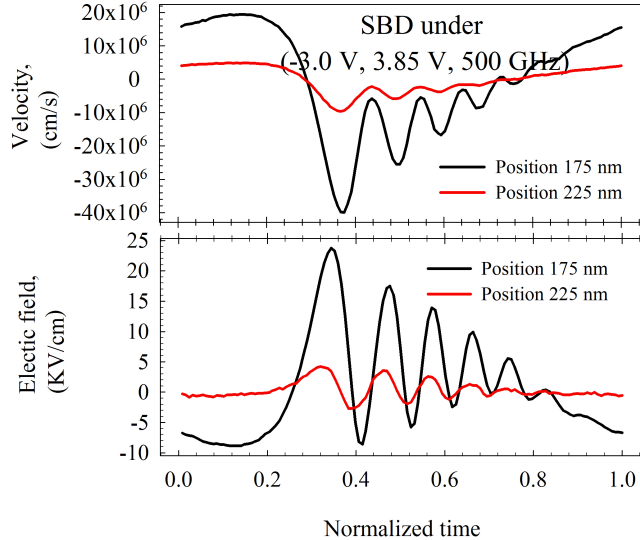


FIG. 7. Time evolution of the electron velocity and the electric field in the neutral regions of the reference SBD (position 175 nm corresponds to the neutral epilayer and 225 nm to the neutral substrate, with the Schottky contact at position 0 nm) under (-3.0 V, 3.85 V, 500 GHz) from MC simulations.

At higher frequencies of the applied signal the first kind of *NHOs* disappears. Only for the reference SBD appears a peak in the spectra at frequencies around 11 THz, see Fig. 6, due to the second kind of oscillations observed in Fig. 3, in accordance with the frequencies calculated from the time domain response, Table III.

D. Internal distributions

The signature of the *NHOs* can be observed in the time evolution of the electron velocity and the electric field. Fig. 7 shows oscillations of these quantities in neutral regions of the reference SBD under (-3.0 V, 3.85 V, 500 GHz), associated to the first kind of *NHOs*.

Under (-3.0 V, 3.85 V, 900 GHz), oscillations of the electron velocity and the electric field appear in the substrate of the reference SBD due to the second kind of *NHOs*, as Fig. 8 shows.

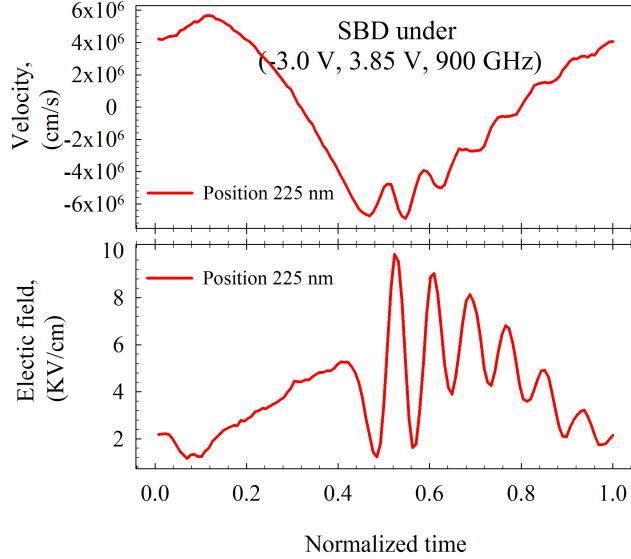


FIG. 8. Time evolution of the electron velocity and the electric field in the neutral substrate region of the reference SBD under $(-3.0 \text{ V}, 3.85 \text{ V}, 900 \text{ GHz})$ from MC simulations. The Schottky contact is at position 0 nm .

III. ANALYTICAL DEVICE MODELING

To describe the electron dynamics and interpret the features of the *NHOs* obtained from MC simulation of Schottky diodes in Section II, this section presents a simple analytical model for the diode. This model is based on the standard depletion approximation to define the width of the depletion region due to the Schottky contact and the momentum balance equation to describe the transport in the non-depleted regions of the diode¹⁷. Drift-diffusion model is not able to predict the generation of the *NHOs*. A description of the *NHOs* based on a lumped element equivalent circuit of the diode is presented. This model might be useful for circuit design.

A. General approach

The Schottky diode is considered a unipolar device and, therefore, hole contributions are neglected. To analyse the current flow through the diode, the structure of the device is divided into three regions, see Fig. 9: (i) The depleted region of the epilayer; (ii) the non-depleted epilayer and (iii) the neutral substrate region. It is assumed that the space charge region is completely depleted and that the height of the potential barrier originated

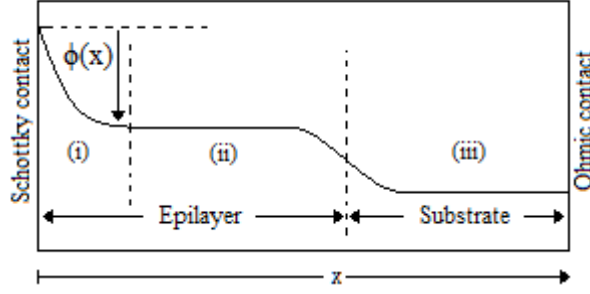


FIG. 9. Sketch of the conduction band of the SBD.

by the $n^+ - n$ homojunction is independent of the applied signal: $\Delta V_{n^+ - n} = (E_{f,s} - E_{f,e})/q$, where $E_{f,i}$ is the Fermi level of the i -region calculated with the Fermi-Dirac statistics for the bulk semiconductor in equilibrium.

The potential across the region (i) considering the full depletion approximation is (see Fig. 9):

$$\phi(x) = V_{bi} - V - \frac{qN_e}{2\epsilon_0\epsilon_r}(\omega - x)^2, \quad (1)$$

where V_{bi} is the built-in voltage of the epilayer, N_e is the epilayer doping concentration, $\epsilon_0\epsilon_r$ is the permittivity of the semiconductor, q the absolute value of the electron charge, V the applied voltage that drops in the depletion region and ω the width of the depletion region at V .

Under time varying conditions, the total current density in the depletion region (and consequently through the SBD) is the sum of the thermionic current density over the Schottky barrier and the displacement current density, that is independent of the position under full depletion approximation:

$$J = J_0(e^{qV/nK_bT} - 1) - qN_e \frac{d\omega}{dt}, \quad (2)$$

where n is the ideality factor and J_0 is the reverse saturation current of the diode. Tunneling current is neglected.

The conduction current density J_i in the non-depleted epilayer ($i = e, J_e$) and the substrate ($i = s, J_s$) assuming constant temperature and neglecting carrier density gradients is described by eq. (3), derived from the Boltzmann transport equation¹⁷.

$$J_i + \tau_i \frac{dJ_i}{dt} = \tau_i \frac{q^2 N_i}{m^*} E_i, \quad i = e, s, \quad (3)$$

where m^* is the effective mass of the electrons in the semiconductor, $\tau_i = m^* \mu_i / q$ the average collision time in the neutral i -regions and μ_i the constant low field electron mobility. This

equation means that the acceleration of the carriers (variation of the conduction current J_e) is finite and introduces a time delay between the action of the electric field and the response of the current^{23,24} (inertia of the carriers). The average collision times, τ_i , are very small, typically on the order of tenths of picoseconds. The term $\tau_i dJ_i/dt$ can be considered as a small perturbation in eq. (3). Drift-diffusion assumes that $\tau_i dJ_i/dt$ is negligible with respect to J_i , and, therefore, the current relation implicates the instantaneous response of the conduction current to the electric field

$$J_i = \frac{q^2 N_i \tau_i}{m^*} E_i, \quad i = e, s. \quad (4)$$

Eq. (4) corresponds to the current relation used in drift-diffusion models (without considering diffusion contributions).

The electric field in the neutral epilayer and substrate E_i , $i = e, s$ is considered independent of the position since we assume that the charge density disappears outside of the depletion region²⁴. Under time varying conditions, the total current in the neutral regions of the SBD is:

$$J_{t,i} = J_i + \epsilon_0 \epsilon_r \frac{dE_i}{dt}. \quad (5)$$

From eq. (1), the relation between the applied voltage V_{app} and ω is:

$$V_{app} = V_{bi} - \frac{qN_e}{2\epsilon_0\epsilon_r} \omega^2 + E_e(L_e - \omega) + E_s L_s. \quad (6)$$

For HSBDs, by imposing the continuity of the current in the epilayer (eqs. (2) and (5)) and eq. (3) for the conduction current in the neutral epilayer, the system of equations for J_e and ω to solve is:

$$\frac{dJ_e}{dt} = \frac{q^2 N_e}{m^*} E_e - \frac{J_e}{\tau_e}, \quad (7a)$$

$$J_0(e^{qV/nK_bT} - 1) - qN_e \frac{d\omega}{dt} = J_e + \epsilon_0 \epsilon_r \frac{dE_e}{dt}, \quad (7b)$$

where E_e is expressed in terms of J_e and ω from eq. (6). We denote these equations by momentum balance (MB) model since they include the momentum balance equation for J_e , eq. (3). If we apply eq. (4) to describe the conduction current in the neutral epilayer, the system of eqs. (7) is reduced to the following equation for the width of the depletion region (denoted by drift diffusion (DD) model):

$$J_0(e^{qV/nK_bT} - 1) - qN_e \frac{d\omega}{dt} = \frac{q^2 N_e \tau_e}{m^*} E_e + \epsilon_0 \epsilon_r \frac{dE_e}{dt}, \quad (8)$$

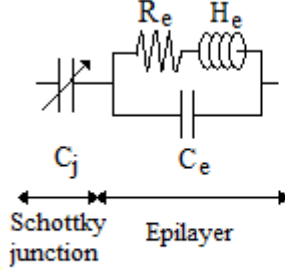


FIG. 10. Equivalent circuit of a HSB D.

where E_e and J_e are expressed in terms of ω from eqs. (6) and (4), respectively.

The generalization of the equations presented in this Section for SBDs with substrate is straight-forward, leading to a system of four independent differential equations for J_e , J_s , ω and E_e . However, this model only predicts the first kind of the *NHOs*, see Section IV.

B. Equivalent circuit model

The performance of the first kind of the *NHOs* can be described by means of a lumped element equivalent circuit (EC model) Fig. 10. The Schottky junction space-charge capacitance is usually approximated by eq. (9) while the nonlinear resistance of the junction is neglected for the varactor operation regimes considered in this paper.

$$C_j = \frac{C_{j0}}{\sqrt{1 - V/V_{bi}}} , \quad (9)$$

where $C_{j0} = A(q\epsilon_0\epsilon_r N_e / (2V_{bi}))^{0.5}$ is the junction capacitance at $V=0$. The relation between the current and the voltage in the neutral region of the epilayer is defined by a simple RLC subcircuit shown in Fig. 10²³. The values of R_e , H_e and C_e are:

$$R_e = \frac{m^* L_e}{N_e q^2 \tau_e A} , \quad (10a)$$

$$H_e = \frac{m^* L_e}{N_e q^2 A} , \quad (10b)$$

$$C_e = \epsilon_0 \epsilon_r \frac{A}{L_e} , \quad (10c)$$

where L_e is the total length of the epilayer and the other parameters meaning as usually. In this model we assume time independent length of the neutral region of the epilayer.

There exists a direct relation between the EC and the MB models. The capacitor C_e in the EC model Fig. 10 accounts for the displacement current in the neutral epilayer of

the MB model $\epsilon_0\epsilon_r dE_e/dt$ eq. (5). On the other hand, the performance of the conduction current J_e described by eq. (3) is represented by the inductance H_e , that accounts for the delayed response of J_e to the electric field (term $\tau_e dJ_e/dt$), and R_e the series resistance of the epilayer.

IV. PHYSICAL INTERPRETATION

The main features of the *NHOs* obtained from MC simulations of Schottky diodes in Section II are analysed in this Section by means of the analytical MB model. We find that this model predicts correctly the first kind of the *NHOs*, but it is required an accurate model of the $n^+ - n$ junction to describe the second kind. Therefore, the analysis of the second kind of *NHOs* presented here is completely based on the results of MC simulations.

A. First kind of the *NHOs*

Section II showed that the first kind of the *NHOs* are common to HSBs and SBDs and they present similar frequencies in both devices. To simplify the analysis of these *NHOs*, this subsection takes as a reference the HSBs. The results presented in this subsection are applicable to the first kind of oscillations in SBDs.

1. Qualitative analysis

Fig. 11 compares the current response of the reference HSB under (-3.0 V, 3.85 V, f), $f=100$ and 300 GHz obtained from the MB, the DD, the EC and the MC models. At 100 GHz, the four models predict the same current response, but at 300 GHz only the MC, the MB and the EC models predict the *NHOs* (the first kind of *NHOs* described in Section II). The comparison of the DD and the MB models shows that it is necessary to include the term $\tau_e dJ_e/dt$ in the conduction current equation (equivalent to H_e in the EC model) to predict the *NHOs*. Therefore, the *NHOs* are the result of coupling the inertial performance of the charge carriers (term $\tau_e dJ_e/dt$) to the nonlinear variation of the depletion region width.

To interpret the nonharmonic oscillations, we compare the performance of the carrier dynamics described by the DD model, where the conduction current responds instantaneously to the electric field, and the MB model that includes the term $\tau_e dJ_e/dt$ in the equation for

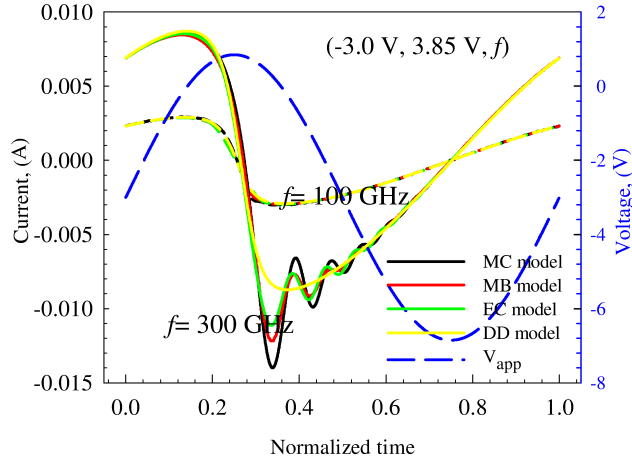


FIG. 11. Current response of the reference HSBD under $(-3.0 \text{ V}, 3.85 \text{ V}, f)$ with $f= 100 \text{ GHz}$ and 300 GHz from the numerical solution of eqs. (7), the EC model, eq. (8) and MC simulations.

the conduction current, eq. (7). Figs. 12 and 13 show the time evolution of the electrical variables (J_e , $\tau_e dJ_e/dt$, σE_e and ω) of the reference HSBD under $(-3.0 \text{ V}, 3.85 \text{ V}, 300 \text{ GHz})$ obtained with the MB and DD models. From the comparison between the response of the two diode models presented in Figs. 12 and 13 and according to the description of the models presented in Subsection III A, we can write the variables of the MB model (denoted by a slash) as the sum of the variables of the DD model (without slash) and a small perturbation: $\tilde{J}_e = J_e + \delta J_e$, $\tilde{\omega} = \omega + \delta\omega$, $\tilde{E}_e = E_e + \delta E_e$. The deviations of $\tilde{\omega}$ from the reference ω of the DD model, Fig. 13, lead to the electric fields δE_e acting to return $\tilde{\omega}$ back to the reference ω , eqs. (7). These forces and electron inertia are responsible for current oscillations.

2. Condition to generate the NHOs

The results presented in Section II show that some conditions have to be satisfied in order to excite the first kind of the *NHOs*. Subsection IV A showed that the term $\tau_e dJ_e/dt$ in the MB model is necessary to generate the oscillations. On the other hand, the current relation, eq. (3), indicates that this term will begin to dominate the response of the SBD when it takes values of the order of J_e . Therefore, we define the ratio between the maximum amplitude of $\tau_e dJ_e/dt$ and the maximum amplitude of J_e in a period of the applied signal ($r = \frac{\tau_e dJ_e/dt}{J_e}$) to determine if the *NHOs* appear in the current response of the diode.

Fig. 14 shows r for the reference HSBD under different applied signals simulated with

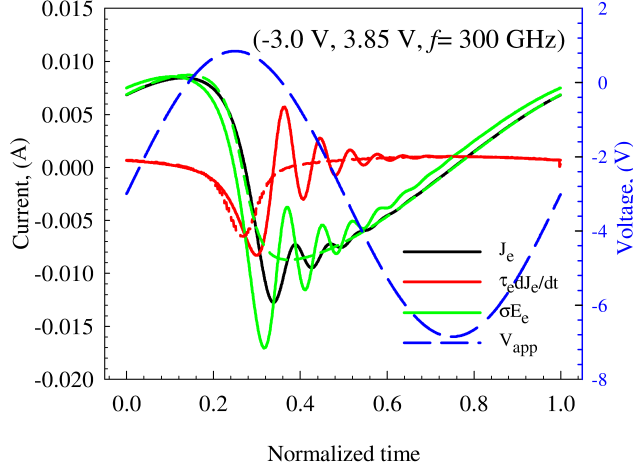


FIG. 12. Time evolution of J_e , $\tau_e dJ_e/dt$ and σE_e for the reference HSB D under applied signal (-3.0 V, 3.85 V, 300 GHz) from the MB model eqs. (7) (continuous lines) and the DD model eq. (8) (dashed lines). In the DD model eq. (8) $J_e = \sigma E_e$, with $\sigma = q^2 N_e \tau_e / m^*$.

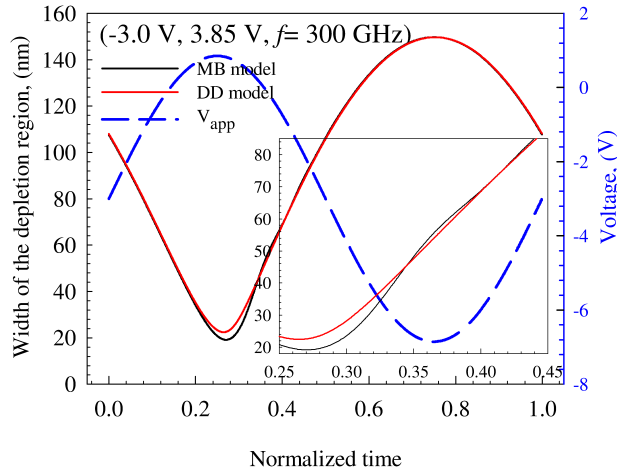


FIG. 13. Time evolution of the width of the depletion region of the reference HSB D under (-3.0 V, 3.85 V, 300 GHz) from the numerical solution of eqs. (7) (black line) and eq. (8) (red line).

the MC method ((-3.0 V, 3.85 V, f), (-3.0 V, 3.0 V, f) and (0.0 V, 0.9 V, f)). In this figure, τ_e has been calculated by MC simulations according to its definition $\tau_e = m^* \mu_e / q = m^* v_e(x, t) / (E_e(x, t) q)$ where the electric field E_e and the electron velocity v_e have been evaluated in neutral regions of the epilayer. The conduction current has been evaluated as $J_e = q n_e(x, t) v_e(x, t)$ where $n_e(x, t)$ is the electron density.

Fig. 14 shows that the ratio r increases with the frequency of the applied signal f^{25} up to a frequency that depends on the applied waveform. For higher frequencies, τ_e decreases

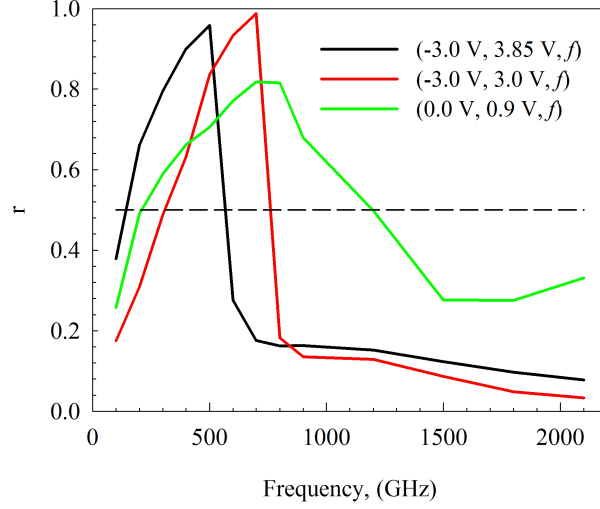


FIG. 14. Dependence of r on the bias point, frequency and amplitude of the applied signal for the reference HSBD simulated with the MC method. The dashed line corresponds to $r=0.5$.

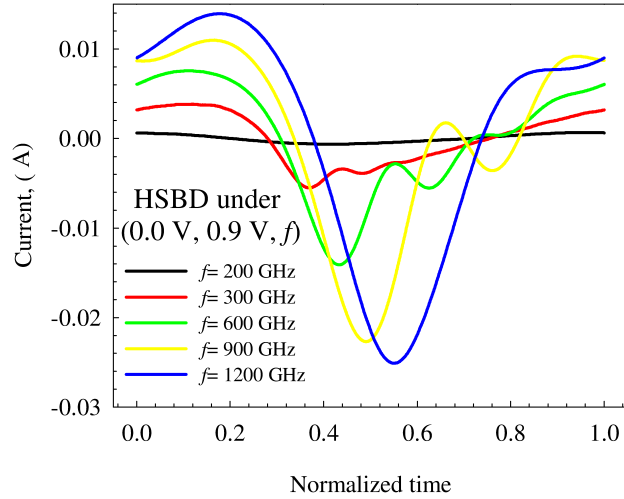


FIG. 15. Current response obtained from the MC simulation of the reference HSBD under $(0.0 \text{ V}, 0.9 \text{ V}, f)$.

because of the increment of the L-intervalley scattering probability, what limits the current flowing in the device (saturation phenomenon²¹) and, therefore, r decreases.

According to the current response obtained from the MC simulation of the reference HSBD under the signals $(-3.0 \text{ V}, 3.85 \text{ V}, f)$, see Fig. 1, $(-3.0 \text{ V}, 3.0 \text{ V}, f)$ and $(0.0 \text{ V}, 0.9 \text{ V}, f)$ -presented in Fig. 15- the first kind of *NHOs* appears for $r > 0.5$. Therefore, it is necessary that the applied signal leads to values of $\tau_e dJ_e/dt$ of the order of J_e in the SBD to excite the *NHOs*.

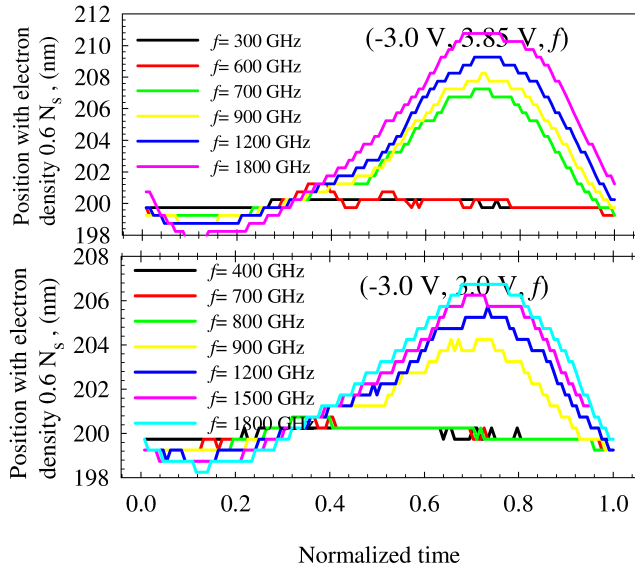


FIG. 16. Time evolution of the position with electron density $0.6 N_s$ from the MC simulation of the reference SBD under $(-3.0 \text{ V}, 3.85 \text{ V}, f)$ and $(-3.0 \text{ V}, 3.0 \text{ V}, f)$ for different frequencies f . The Schottky contact is at position 0 nm.

B. Second kind of $NHOs$

From Section II, we know that a new kind of $NHOs$ is generated in the reference SBD under applied signals $(-3.0 \text{ V}, 3.85 \text{ V}, f)$ with f higher than 600 GHz. Fig. 16 shows how the position of the device with electron density 0.6 times the doping of the substrate N_s evolves under the signals $(-3.0 \text{ V}, 3.85 \text{ V}, f)$ and $(-3.0 \text{ V}, 3.0 \text{ V}, f)$. The second kind of $NHOs$ appears when the $n^+ - n$ junction is modulated by the applied signal. Therefore, its origin is equivalent to the origin of the first kind of oscillations (Subsection IV A 1), i.e. the modulation of the nonlinear $n^+ - n$ junction²⁶ by the inertial motion of the charge carriers in the substrate and the epilayer.

Fig. 17 presents the electric field profiles at different normalized times for the reference SBD under $(-3.0 \text{ V}, 3.85 \text{ V}, f)$ for $f = 600 \text{ GHz}$ and 700 GHz . The high electric field induced in the epilayer of the SBD, see Fig. 17, leads to a high occupation of the upper valleys of the semiconductor (higher than 85 %) and to the enhancement of the $n^+ - n$ potential barrier.

Since the analytical models presented in Section III do not include an accurate model for the $n^+ - n$ transition, the MB and the EC models do not predict the second kind of $NHOs$.

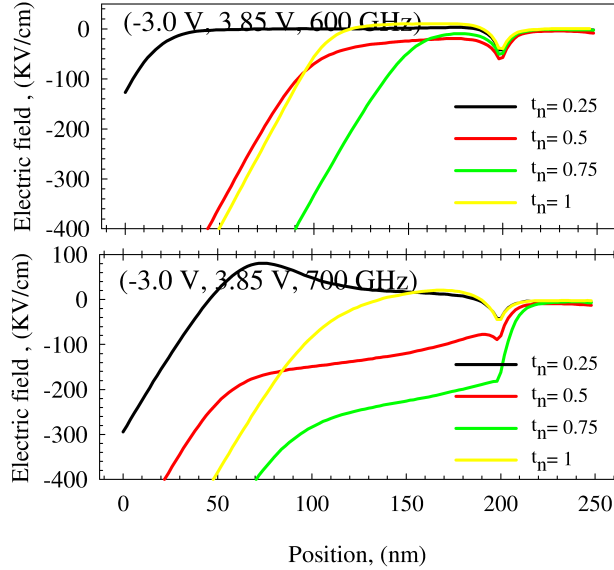


FIG. 17. Electric field profiles of the reference SBD under $(-3.0 \text{ V}, 3.85 \text{ V}, f)$ with $f= 600 \text{ GHz}$ and 700 GHz , obtained from MC simulations at different normalized times t_n . Position 0 corresponds to the Schottky contact.

V. CONCLUSIONS

The Monte Carlo method has been used to show the generation of two kind of non-harmonic oscillations in the current response of Schottky diodes. We have given a physical interpretation of these oscillations based on the modulation of the nonlinearities of the diode by the delayed response of the charge carriers to the electric field in the neutral regions of the SBD. While the first kind of oscillations is due to the modulation of the nonlinear capacitance of the Schottky junction, the second kind is generated by the modulation of the nonlinearity of the $n^+ - n$ junction when the applied signal leads to strong electric fields in the epilayer that increment the potential barrier generated at the $n^+ - n$ junction.

The analytical models applied to describe the current in the diode have shown that the condition to generate the first kind of *NHOs* involves values of $\tau_e dJ_e/dt$ of the order of J_e .

ACKNOWLEDGMENTS

This work was supported by the Junta de Castilla y Leon under project GR270, Spanish National Research and Development Program under projects TEC2008-02148, TEC2010-

15413, TEC2011-28683-C02-01, TeraSense (Consolider- Ingenio 2010, CDS2008-00068) and European Commission under projects RooTHz (ICT-2009-243845), MIDAS (FP7-SPACE-2009-1 242334).

REFERENCES

- ¹P. H. Siegel, *IEEE Trans. Microwave Theory Tech.* **50**, 910 (2002).
- ²T. W. Crowe, W. L. Bishop, D. W. Porterfield, J. L. Hesler, and I. Weikle, R. M., *IEEE J. Solid-State Circuit* **40**, 2104 (2005).
- ³A. Maestrini, B. Thomas, H. Wang, C. Jung, J. Treuttel, Y. Jin, G. Chattopadhyay, I. Mehdi, and G. Beaudin, *C. R. Phys.* **11**, 480 (2010).
- ⁴G. Chattopadhyay, *IEEE Trans. Terahertz Sci. Tech.* **1**, 33 (2011).
- ⁵P. Shiktorov, E. Starikov, V. Gruzinskis, S. Perez, T. Gonzalez, L. Reggiani, L. Varani, and J. C. Vaissiere, *IEEE Electron Device Lett.* **25**, 1 (2004).
- ⁶U. V. Bhapkar, *Monte Carlo Simulation of Gallium Arsenide Schottky Diodes for Terahertz Frequencies*, Ph.D. thesis, UNIVERSITY OF VIRGINIA. (1995).
- ⁷I. R. Gatland, *Am. J. Phys.* **59**, 155 (1991).
- ⁸A. Y. Spasov, *Electron. Lett.* **4**, 365 (1968).
- ⁹E. H. Hellen and M. J. Lanctot, *Am. J. Phys.* **75**, 326 (2007).
- ¹⁰A. Boff, J. Moll, and R. Shen, in *ISSCC Dig. Tech. Papers*, Vol. III (1960) pp. 50 – 51.
- ¹¹J. Moll, S. Krakauer, and R. Shen, *Proc. IRE* **50**, 43 (1962).
- ¹²M. Lin, Y. Zhang, and Z. Zhang, in *CPEM* (2010) pp. 728 –729.
- ¹³A. Zhu, F. Sheng, and A. Zhang, in *ICUWB*, Vol. 2 (2010) pp. 1 –4.
- ¹⁴S. Oh and D. Wentzloff, in *ICUWB* (2011) pp. 63 –67.
- ¹⁵P. P. Labs, *Microw. J.* **49**, 278 (2006).
- ¹⁶M. Kintis, X. Lan, F. Fong, D. Sawdai, K. Loi, K. Kono, and A. Gutierrez, *IEEE Microw. Wirel. Compon. Lett.* **17**, 454 (2007).
- ¹⁷S. Selberherr, *Analysis and simulation of semiconductor devices* (Springer-Verlag, 1984).
- ¹⁸M. V. Fischetti and S. E. Laux, *Phys. Rev. B* **38**, 9721 (1988).
- ¹⁹N. S. Mansour, K. Diff, and K. F. Brennan, *J. Appl. Phys.* **70**, 6854 (1991).
- ²⁰The results provided by the MC simulations have been obtained by averaging 250 simulated periods of the applied signal.

- ²¹E. L. Kolberg, T. J. Tolmunen, M. A. Frerking, and J. R. East, *IEEE Trans. Microwave Theory Tech.* **40**, 831 (1992).
- ²²J. Grajal, V. Krozer, E. Gonzalez, F. Maldonado, and J. Gismero, *IEEE Trans. Microwave Theory Tech.* **48**, 700 (2000).
- ²³K. S. Champlin, D. B. Armstrong, and P. D. Gunderson, *Proc. IEEE* **52**, 677 (1964).
- ²⁴B. L. Gelmont, D. L. Woolard, J. L. Hesler, and T. W. Crowe, *IEEE Trans. Electron Devices* **45**, 2521 (1998).
- ²⁵ $J \simeq -qN_e d\omega/dt$ where $\omega \sim (2\epsilon_0\epsilon_r(V_{bi} - V_{app})/(qN_e))^{0.5}$ and $r \sim 2\pi f\tau_e((V_{bi} - V_0)/(V_{bi} - V_0 - V_1))^{0.5}$.
- ²⁶H. S. Abdel-Aty-Zohdy, P. S. Gudem, and S. D. MacFarlane, in *Proc. 35th Midwest Symp. Circuits and Systems* (1992) pp. 416–420.